REPORT TITLE:

ACTIVE CATHODES FOR SUPER-HIGH POWER DENSITY SOLID OXIDE FUEL CELLS THROUGH SPACE CHARGE EFFECTS

DISCLAIMER:

This report was prepared as an account of work sponsored by an agency of the United States Government. Neither the United States Government nor any agency thereof, nor any of their employees, makes any warranty, express or implied, or assumes any legal liability or responsibility for the accuracy, completeness, or usefulness of any information, apparatus, product or process disclosed, or represents that its use would not infringe privately owned rights. Reference herein to any specific commercial product, process, or service by trade name, trademark, manufacturer, or otherwise does not necessarily constitute or imply its endorsement, recommendation, or favoring by the United States Government or any agency thereof. The views and opinions of authors expressed herein do not necessarily state or reflect those of the United States Government or any agency thereof.

ABSTRACT

This report summarizes the work done during the sixth quarter of the project. Effort was directed in three areas: (1) Further development of the model on the role of connectivity on ionic conductivity of porous bodies, including the role of grain boundaries and space charge region. (2) Calculation of the effect of space charge and morphology of porous bodies on the effective charge transfer resistance of porous composite cathodes. (3) The investigation of the three electrode system for the measurement of cathodic polarization using amperometric sensors.

TABLE OF CONTENTS

INTRODUCTION

It is known that electrode transport properties and morphology have a profound effect on electrode polarization and thus on solid oxide fuel cell (SOFC) performance [1-4]. Recent work has shown that a large part of the polarization loss is associated with the cathode [5, 6]. In addition to the morphological effect, it is also known that the ionic conductivity of cathode has a large effect on cathodic polarization. This is expected to be the case regardless of whether the cathode is a mixed ionic electronic conducting (MIEC) composite cathode or a MIEC single-phase cathode. While the focus of the work discussed in this report is on composite cathodes such as LSM + YSZ, the general features are applicable to MIEC cathodes such as LSC, LSF, and LSCF. It is assumed that the electronic conductivity of the cathode is high enough, not to be a limiting factor. This is usually a good assumption with materials such as LSM and LSC, which have electronic conductivities over the temperature of interest between ~200 and 1000 S/cm. By contrast, the ionic conductivity of either YSZ or ceria or LSGM is well below 1 S/cm at similar temperatures. Even with the possible use of bismuth oxide for the cathode, the ionic conductivity is still much lower than the electronic conductivity of the electrocatalyst. The grain size also has a large effect on conductivity [7]. It is desired that the cathode microstructure close to the electrolyte be as fine as possible. When the particle size is very fine, there can be a significant effect of space charge on transport [8-13]. The effect of space charge can be potentially quite large in ionic conductors. It could either increase conductivity, or could decrease it. It is desired that the space charge be such that it enhances ionic conductivity of porous bodies. It is possible, however, that space charge effects are actually detrimental in many oxygen ion conductors. In such a case, the approach should be to seek to lower these effects. In the former case, it is desired that the cathodes be annealed at lower temperatures so as to increase the Debye length. In the latter case, it is desired that the cathodes be annealed at higher temperatures so as to suppress the Debye length. Work done to date suggests that in most materials of interest, the space charge tends to lower ionic conductivity. This implies that the cathodes need to be annealed at higher temperatures. The implication is that there are conflicting requirements from the standpoint of microstructural issues and space charge related issues, insofar as cathode polarization resistance is concerned.

One area in which space charge effects can be significant is the effect of grain size on conductivity. Another one of great importance is the morphology of the cathode, and especially that of the ionic conductor in composite cathodes. When ionic current has to flow from one grain to the adjacent grain, it is necessary that narrowing in the neck region be accounted for. In the past reports, preliminary results on both theoretical analysis and experimental aspects were reported. In this report, further development of the model is described, along with the results of calculations. In addition, the effect of space charge on the cathodic polarization resistance is calculated.

One of the critical issues concerns the measurement of cathodic overpotential. The usual approach is to deposit a prospective cathode on a YSZ disc as a working electrode, and apply a DC voltage across the working and the counter electrodes. The current vs. overpotential (with respect to a symmetrically placed reference electrode) are measured

as a function of applied voltage. Our theoretical work shows that this approach could be seriously flawed. Experimental work has been conducted using amperometric sensors, which show that bulk of the current is due to the decomposition of the electrolyte (or the generation on nonstoichiometry), which leads to an overestimation of the cathodic activity. Thus, the only realistic method of assessing cathode performance is through actual fuel cell testing.

EXECUTIVE SUMMARY

Solid oxide fuel cells (SOFC) can operate over a wide temperature range, from ~600 to 1000°C, and can use a variety of hydrocarbon fuels, once appropriately processed. The current target for SOFC is about 800°C, although efforts are presently underway to lower the operating temperature below 700°C. The largest voltage loss (polarization) in SOFC is known to occur at the cathode, especially at relatively low temperatures (<800°C). There are two types of cathodic polarizations: (1) Concentration polarization – that associated with gas transport. (2) Activation polarization – that associated with the occurrence of the overall electrochemical cathodic reaction of charge transfer. The former is relatively small, as long as the cathode is thin and has sufficient porosity [14]. The latter is the dominant one, and depends upon a number of microstructural and intrinsic – fundamental, parameters. This research aims to address cathodic activation polarization. Specifically, this research aims to lower the cathodic polarization by cathode modification through space charge effects. Our prior work has shown that the effective cathodic polarization resistance depends upon the following factors. (1) The particle size of the ionic conductor in a composite cathode, comprising a two phase, porous, contiguous mixture of an ionic conductor and an electrocatalyst – the latter being an electronic conductor. In general, the smaller the particle size of the ionic conductor, the lower is the cathodic activation polarization. (2) The ionic conductivity of the ionic conductor in the cathode also has a significant effect – the higher the ionic conductivity, the lower is the cathodic polarization. (3) Intrinsic charge transfer resistance – the lower the intrinsic charge transfer resistance, the lower is the cathodic activation polarization.

The above factors themselves depend upon additional fundamental parameters. It is known that in the majority of the ionic conductors, the smaller the grain size, the higher is the net resistivity. This is attributed to grain boundaries, which usually offer resistance to ion transport. Part of this resistance is attributable to space charge effect, which in some materials (e.g. YSZ) tends to lower oxygen vacancy concentration near grain boundaries. Depending upon the dopant type and amount, it is in principle possible to actually enhance the oxygen vacancy concentration near grain boundaries. If this can be achieved, significant lowering of cathodic polarization can occur. This research aims to identify fundamental parameters, which tend to increase oxygen vacancy concentration near grain boundaries. This is expected to depend upon the chemistry of the material as well as processing. In cases where the effect of space charge decreases ionic conductivity, a judicious choice of thermal treatment procedures may mitigate this detrimental effect.

The other factor involves the nature of inter-particle necks. If the contact between particles is narrow (small), the overall resistance can be large, leading to high cathodic polarization. During the previous reporting periods, the effect of inter-particle neck size on total conductivity of porous bodies was theoretically analyzed, and experimental results were presented. The results showed that the neck size between particles has a profound effect on ionic conductivity. Specifically, it was shown that for highly porous samples of identical porosities (~50%), the absolute value of conductivity was ~75 times higher in samples with sufficiently large neck sizes (good connectivity) as compared to samples with small neck sizes (poor connectivity). It is to be noted that this has profound influence on cathode

7

polarization. In the subsequent report (Third quarterly), the effect of grain boundaries was also included. However, the effect included was only that of the structural part of the grain boundary. It is known that the effect of space charge can extend far beyond the structural part of the grain boundary. In fourth quarterly report, results of further model development were included, wherein the effect of space charge region was explicitly included. Three cases have been considered: Space charge region having higher, equal to, and lower resistivity compared to the bulk grains. The effect of neck size on the effective resistivity has been explicitly calculated. In this report, the model is extended to include the effects of space charge and morphology on the polarization resistance of composite electrodes.

Experimental work has been conducted on modified amperometric sensors. The objective was to determine the validity of the three electrode system. By constructing YSZ-based amperometric sensors, current vs. voltage characteristics were measured. Since the net influx of oxygen through the diffusion hole of the sensor was dictated by the diffusion hole geometry, any excess current observed cannot be due to the cathodic reaction, and must be due to decomposition or the development of nonstoichiometry. It was observed that under an applied voltage of ~2.2 V, the current due to the noncathodic effects was greater by an order of magnitude than that due to the cathodic reaction. Such effects are expected to prevail in the three electrode system when used under an applied DC bias. The implication is that the three electrode system may grossly overestimate catthodic activity, and is not a reliable technique.

EXPERIMENTAL

During this reporting period, efforts were directed in the following areas.

1. Extension of the theoretical analysis of ionic conduction in porous bodies, including the role of structural part of grain boundaries and the effect of space charge region on the effective resistivity. Some of the calculations were repeated with different values of parameters.

2. The model was extended to estimate the polarization resistance of porous composite cathodes, by incorporating the effects of neck morphology and space charge.

3. Modified amperometric sensors with YSZ electrolyte discs were made and tested.

4. Theoretical analysis of the modified amperometric sensors was conducted. The analysis shows that the three electrode system may grossly overestimate cathodic activity, and is not a reliable technique.

Detailed experimental procedure used for making and testing amperometric sensors is described below.

Cylinders of YSZ (8 mol.% Y_2O_3-stabilized zirconia) of approximate dimensions: ~2 cm outside diameter x 2.2 cm length x 0.2 cm thickness were fabricated by a conventional process comprising pressing of YSZ powder followed by sintering in air at 1450^oC for 2 hours. Discs of YSZ of approximate dimensions, 2.5 cm diameter x 0.1 to 0.2 cm in thickness were similarly fabricated. In one of the discs (of thickness ~0.18 cm), a hole of ~250 micron diameter was drilled in the center of the disc. On the other YSZ disc, platinum electrodes were applied using platinum paste, followed by firing at 1000^oC in air. The electrode area was 2 cm^2. In addition, a platinum wire reference electrode was positioned along the circumference of the disc as shown in Figure 1. Two platinum leads were attached to the two electrodes. On the YSZ cylinder, two sets of platinum electrodes were applied near the two ends of the cylinder, one close to the diffusion hole (4 mm from the disc with the diffusion hole), and the other close to the YSZ disc with platinum electrodes (4 mm from the YSZ disc with electrodes). The distance between the two potentiometric sensors (S1 and S2) was 14 mm. Platinum wires were also bonded to the two sets of platinum electrodes. The two discs were then glass-bonded to the cylinder, making sure that the platinum leads were taken out through the glass seals, and the seals were hermetic. The two sets of platinum electrodes on the YSZ cylinders served as potentiometric sensors. The leads connected to the YSZ disc with platinum electrodes served as the current leads. This completes the fabrication of an amperometric sensor with two sets of potentiometric sensors applied on the YSZ cylinder. Figure 1 shows a schematic of the sensor.

A typical sensor was then heated in air to 800^oC and a DC voltage was applied across the two platinum electrodes deposited on the YSZ disc with the positive lead connected to the outside electrode. The corresponding current was measured. Under the action of the applied voltage,

oxygen from the sensor chamber was pumped out, thus lowering the p_{O_2} in the chamber. This established a flux of oxygen from the ambient, through the diffusion hole, into the cylinder. In steady state over the plateau region, the net flux of oxygen into the cylinder through the diffusion hole corresponds to the net current measured in the external circuit. The measurement of Nernst potentials across the two potentiometric sensors deposited on the YSZ cylinder provides magnitudes of the local p_{O_2}, one close to the diffusion hole, namely $p_{O_2}^{S_1}$, and the other close to the inner electrode (cathode) on the YSZ disc, namely $p_{O_2}^{S_2}$. The measurements were conducted over a wide range of applied voltages, ranging between 0 and ~2.5 V, which covers the initial region, the plateau region, and the post-plateau region of rapidly rising current, as depicted in the schematic of Figure 2.

RESULTS AND DISCUSSION

The Effect of Grain Boundaries on Ionic Conductivity of Porous Bodies: The Effect of Space Charge; Further Model Development: The Estimation of the Effective Polarization Resistance:

Figure 3 shows the geometry used for calculations. This is the same geometry shown in the last two quarterly reports. Calculations were conducted over a wide range of parameters. Figure 4(a) shows the calculated resistance (one half of a grain) of porous YSZ as a function of grain size and neck size at 650°C using the following parameters: ρ_g = 76 Ωcm, ρ_{gb} = 50 Ωcm, ρ_s = 14520 Ωcm, λ = 2 nm, and δ_{gb} = 0.4 nm. These values were obtained from the literature [15]. For all calculations, the intrinsic charge transfer resistance, R_{ct} was chosen to be 2 Ωcm^2. Note that at small values of the neck, the resistance of the grain is rather large, due to the constriction effect. Figure 4(b) shows the corresponding effective resistivity of the porous YSZ sample as a function of grain size and neck size. Figure 4(c) gives the estimated effective polarization resistance of composite cathodes at 650°C. Note that for the values assumed, the polarization resistance varies between ~2 Ωcm^2 for large grains and small necks to ~0.5 Ωcm^2 for small grains and large necks. Figures 5(a) through 5(c) show the results of calculations at 700°C. Note that effective polarization resistance varies between ~1.4 Ωcm^2 for large grains and small necks to ~0.3 Ωcm^2 for small grains are large necks. The values of parameters used were as follows: ρ_g = 41 Ωcm, ρ_{gb} = 40 Ωcm, ρ_s = 7244 Ωcm, λ = 2 nm, and δ_{gb} = 0.4 nm. Figures 6(a) through 6(c) show similar calculations at 750°C, wherein the assumed values are: ρ_g = 23 Ωcm, ρ_{gb} = 20 Ωcm, ρ_s = 3878 Ωcm, λ = 2 nm, and δ_{gb} = 0.4 nm. Note that the effective polarization resistance varies between ~1.0 Ωcm^2 for large grains and small necks to ~0.2 Ωcm^2 for small grains are large necks. Finally, Figures 7(a) through 7(c) show similar calculations at 800°C, wherein the assumed values are: ρ_g = 14 Ωcm, ρ_{gb} = 10 Ωcm, ρ_s = 2250 Ωcm, λ = 2 nm, and δ_{gb} = 0.4 nm. Note that effective polarization resistance varies between ~0.8 Ωcm^2 for large grains and small necks to ~0.15 Ωcm^2 for small grains are large necks. These

calculations thus show the profound effects of morphology and space charge on the effective polarization resistance. Experimental work is currently underway to verify these predictions by conducting out of cell measurements, under no applied DC bias. These will be reported in later reports.

Amperometric Sensors, Electrolyte Stability and Issues Concerning the Three Electrode System: Figure 8 shows the measured current (linear scale) as well as the calculated current (based on the sensor diffusion current equation) as a function of applied voltage for sensor 1. The measured and the calculated currents are in good agreement over the plateau region. Beyond an applied voltage of ~1.7, the measured current increases. At higher applied voltages (above about 2 V), the current rapidly rises, and is considerably greater than the calculated current. This excess current is due to electrolyte decomposition, and/or the development of nonstoichiometry, and is not attributable to the cathodic reaction at electrode I, namely $^1/_2O_2 + 2e' \rightarrow O^{-2}$. Figure 8 shows that the current that can be attributed to the cathodic reaction in this case is only about ~6 mA. For an applied voltage above ~1.9 V, the actual current rapidly rises. Note that the actual current for an applied voltage of 2.2 V is ~90 mA, but only ~6 mA is due to the cathodic reaction. Thus, in this case if all of the current is attributed to the cathodic current, one would effectively overestimate the cathodic activity by more than an order of magnitude. In the amperometric sensor, the geometry of the sensor allows one to precisely determine what the cathodic current is. In the three electrode system, in which there is no barrier hole, it is impossible for one to know how much is the cathodic current and how much is due to electrolyte decomposition or nonstoichiometry development. In order to illustrate this point, Figure 9 shows a schematic of the three electrode system. The working electrode is a prospective cathode, which is porous and of a finite thickness. The net cathodic current may be limited by the porosity, thickness, and the oxygen partial pressure. However, under an applied DC bias, the chemical potential of oxygen, μ_{O_2}, can be considerably lowered just inside the electrolyte, thus leading to local decomposition and/or the development of nonstoichiometry. Figure 10 shows the anticipated variation of the chemical potential of oxygen. The present results thus demonstrate that the three electrode system may grossly overestimate the cathodic activity. Thus, in general, caution must be exercised in using the three electrode system for the measurement of current – overpotential relationships. Details will be described in future reports and manuscripts that will be prepared for publication.

CONCLUSIONS

In this report, the model was developed to include the effect of space charge on transport properties of porous ionic conductors. The effective resistivity and effective polarization resistance were estimated for YSZ-based composite cathodes over a range of temperatures from 650 to 800°C. The results show that the cathode microstructure should consist of fine grains and large necks in order to minimize cathodic activation polarization. The effect of space charge was explicitly included.

Amperometric sensors were made and tested. The results show that the actual current far exceeds the cathodic current at an applied voltage in excess of 1.9 V. At 2.2 V, most of

the current is due to nonstoichiometry development or decomposition. These results show that the three electrode system should be used with caution.
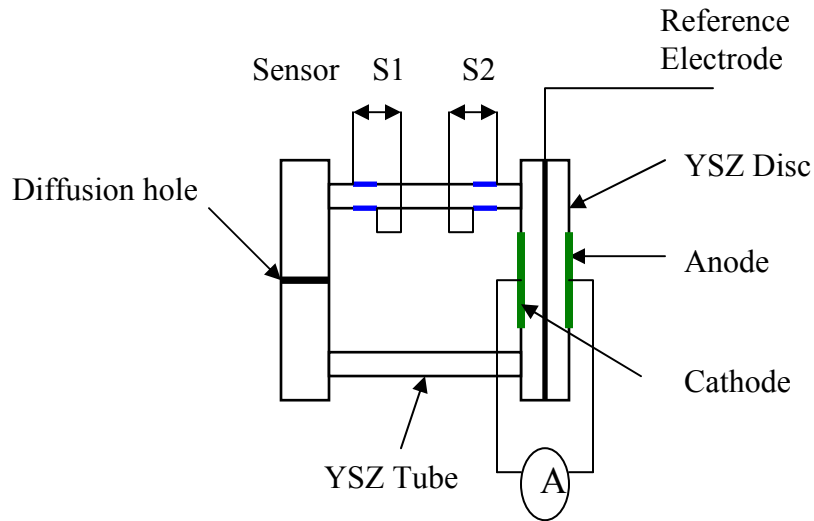

Figure 1: A schematic of the amperometric sensors fabricated and tested, showing the locations of the two potentiometric sensors S1 and S2, for the measurements of $p_{O_2}^a$ and $p_{O_2}^b$.
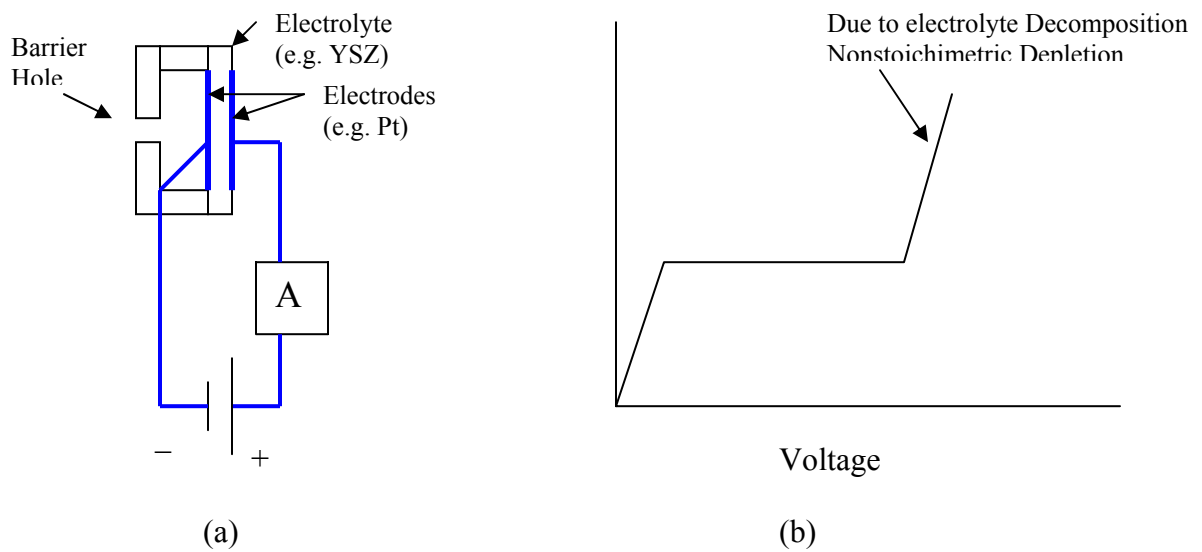
Figure 2: (a) A schematic of an amperometric oxygen sensor. (b) A schematic showing current vs. voltage behavior. The plateau region, which results due to the transport limit imposed by the diffusion hole, corresponds to the oxygen partial pressure in the atmosphere being tested. Increasing current at higher voltages, beyond the plateau region, is due either to the development of nonstoichiometry or decomposition just under the negative electrode, or both.
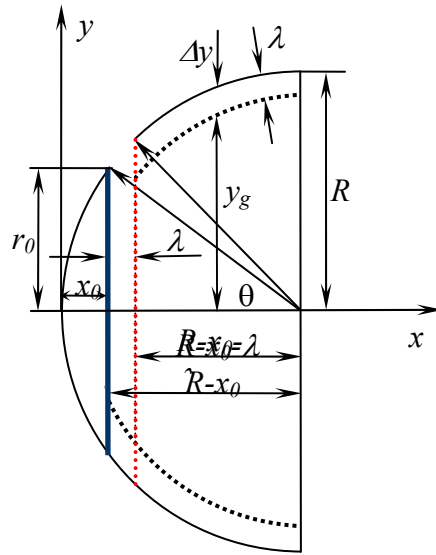
Figure 3: A schematic of the geometry used for the estimation of the role of particle geometry and space charge on the net resistance per grain, and the effective ionic resistivity of porous bodies.

Materials: 8YSZ, Temp: 650 °C
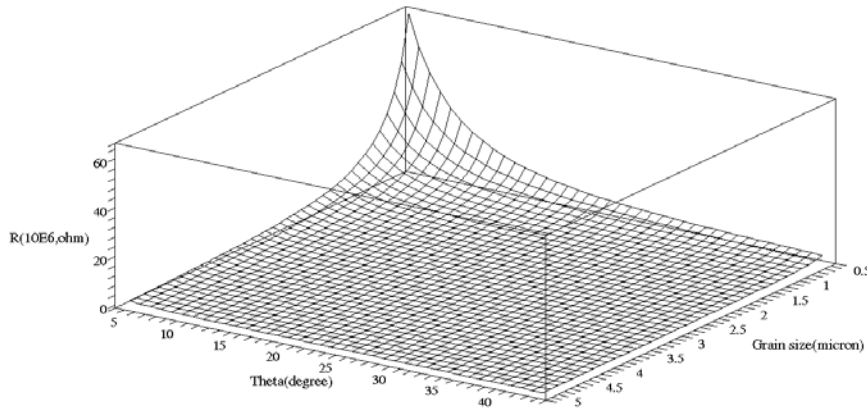Grain =76, space charge=14520 grain boundary=50, λ=4/2 nm, δ$_{gb}$= 0.8/2 nm
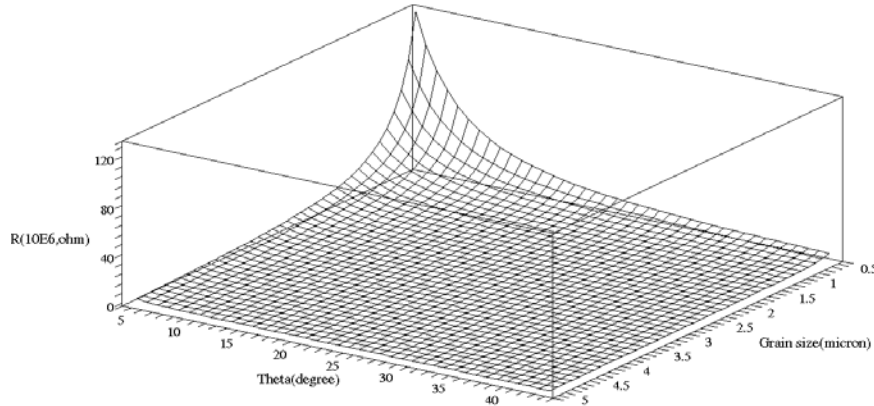
Figure 4(a): Resistance of half a grain (with half grain boundary) as a function of angle (relative neck size) and grain size for YSZ at 650°C.
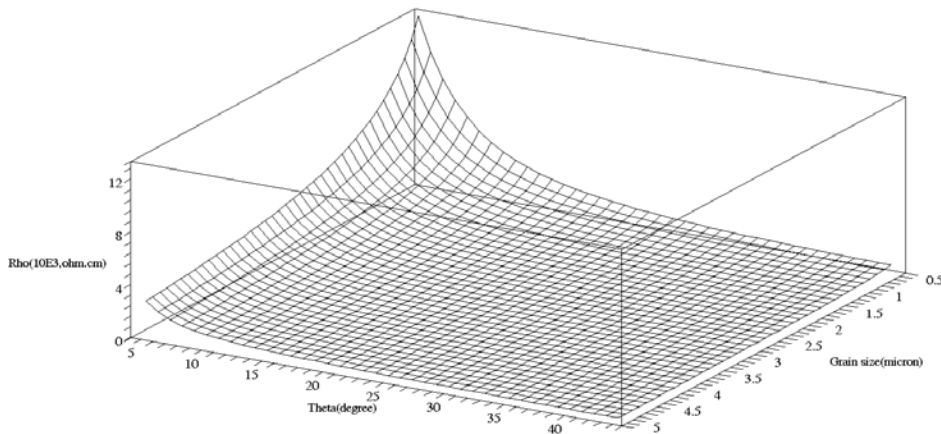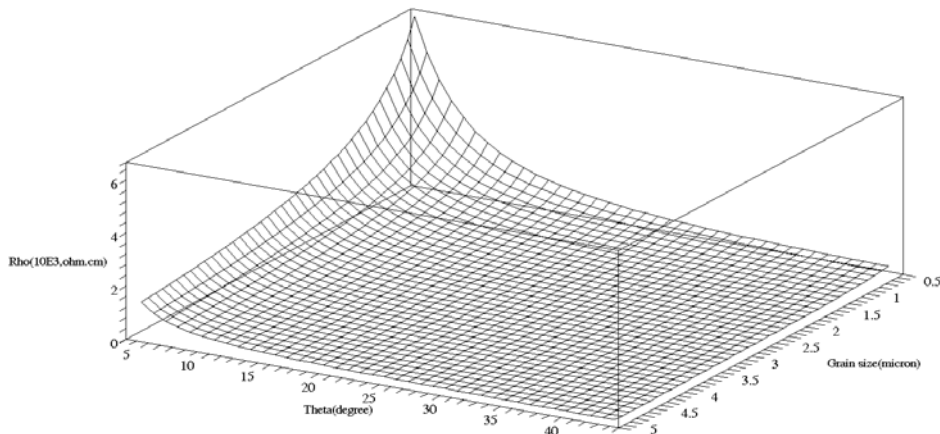

Figure 4(b): Effective resistivity of porous YSZ as a function of angle (relative neck size) and grain size for YSZ at 650°C. Note that the resistivity also rises sharply at small angles (narrow necks).
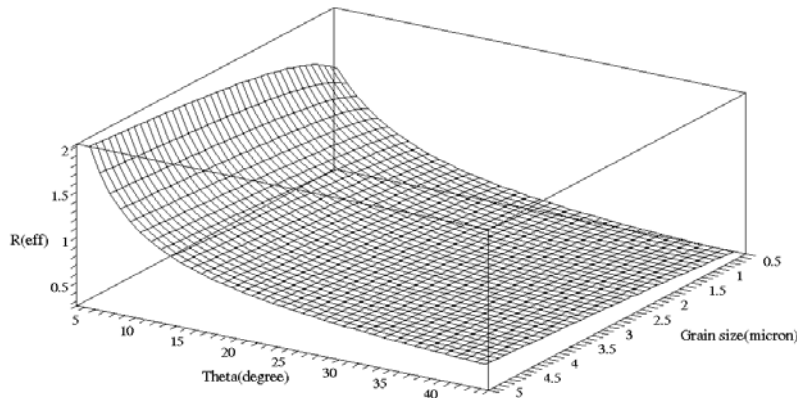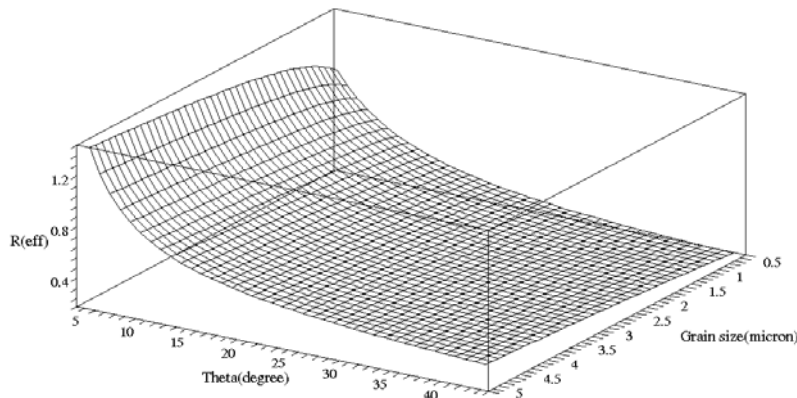

Figure 4(c): Estimated effective polarization resistance at 650°C for an assumed value of the intrinsic charge transfer resistance. Note that fine grains and large neck gives low polarization resistance of composite cathodes.

15

Materials: 8YSZ, Temp: 700 °C
Grain =41, space charge=7244 grain boundary=40, λ=4/2 nm, δ_{gb}= 0.8/2 nm
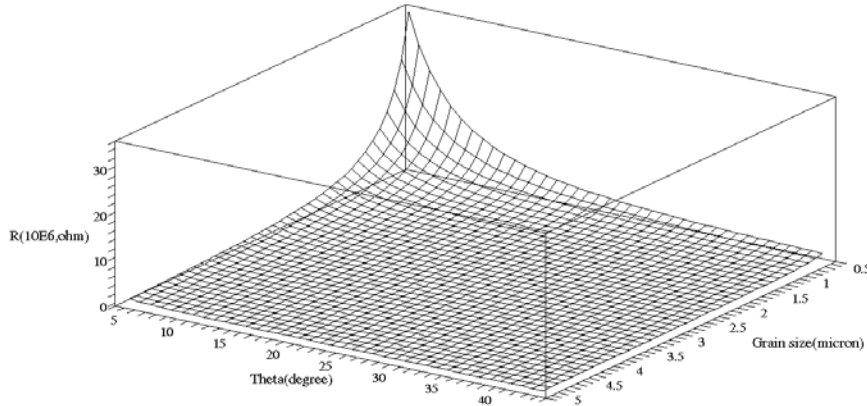

Figure 5(a): Resistance of half a grain (with half grain boundary) as a function of angle (relative neck size) and grain size for YSZ at 700°C.

Figure 5(b): Effective resistivity of porous YSZ as a function of angle (relative neck size) and grain size for YSZ at 700°C. Note that the resistivity also rises sharply at small angles (narrow necks).

Figure 5(c): Estimated effective polarization resistance at 700°C for an assumed value of the intrinsic charge transfer resistance. Note that fine grains and large neck gives low polarization resistance of composite cathodes.

Materials: 8YSZ, Temp: 750 ^{o}C

Grain =23, space charge=3878 grain boundary=20, λ=4/2 nm, δ_{gb}= 0.8/2 nm

Figure 6(a): Resistance of half a grain (with half grain boundary) as a function of angle (relative neck size) and grain size for YSZ at 750°C.
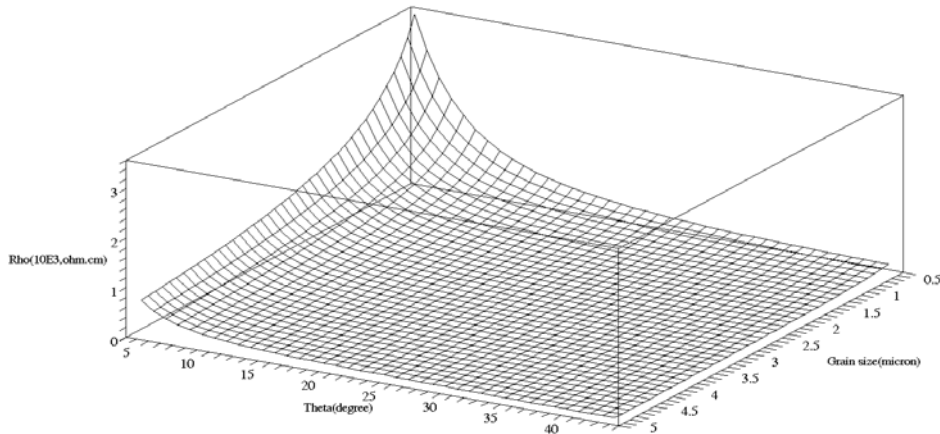

Figure 6(b): Effective resistivity of porous YSZ as a function of angle (relative neck size) and grain size for YSZ at 750°C. Note that the resistivity also rises sharply at small angles (narrow necks).
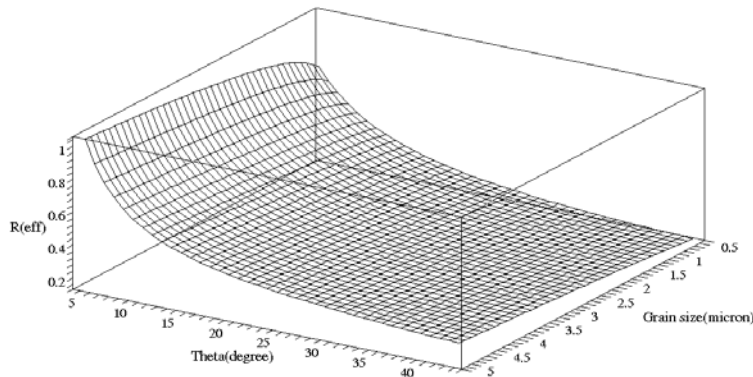

Figure 6(c): Estimated effective polarization resistance at 750°C for an assumed value of the intrinsic charge transfer resistance. Note that fine grains and large neck gives low polarization resistance of composite cathodes.

Materials: 8YSZ, Temp: 800 $^\circ$C
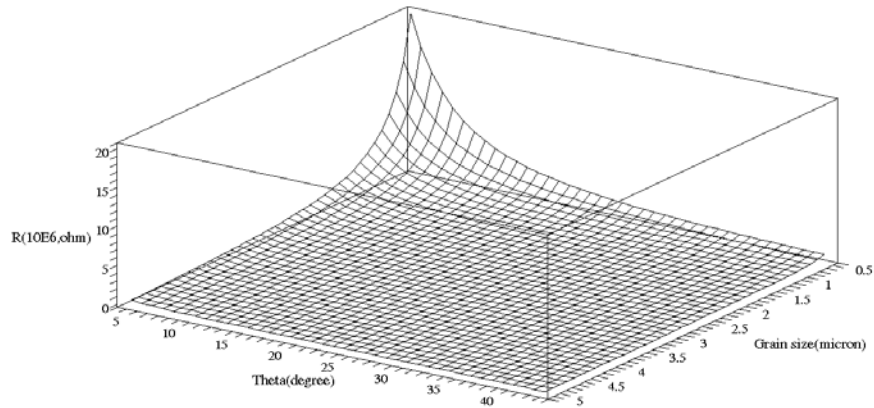Grain =14, space charge=2250 grain boundary=10, λ=4/2 nm, δ_{gb}= 0.8/2 nm

Figure 7(a): Resistance of half a grain (with half grain boundary) as a function of angle (relative neck size) and grain size for YSZ at 800°C.
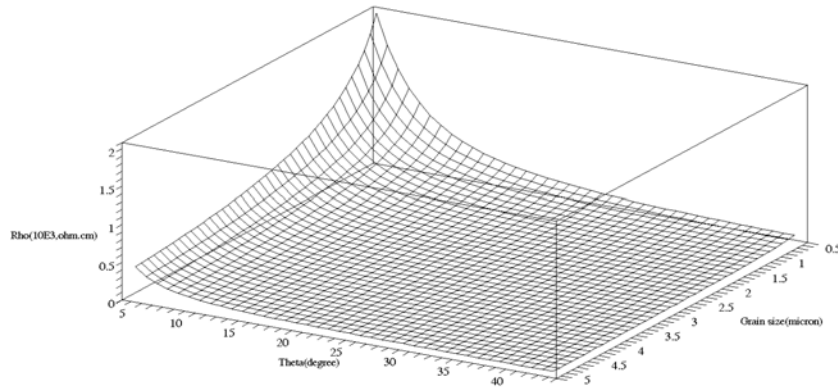

Figure 7(b): Effective resistivity of porous YSZ as a function of angle (relative neck size) and grain size for YSZ at 800°C. Note that the resistivity also rises sharply at small angles (narrow necks).
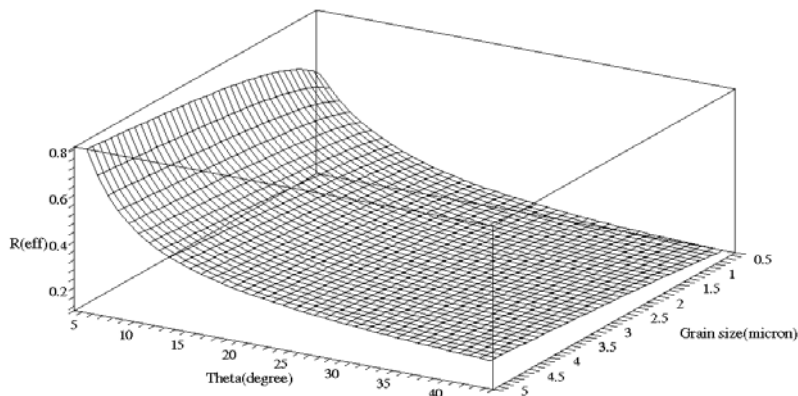

Figure 7(c): Estimated effective polarization resistance at 750°C for an assumed value of the intrinsic charge transfer resistance. Note that fine grains and large neck gives low polarization resistance of composite cathodes.
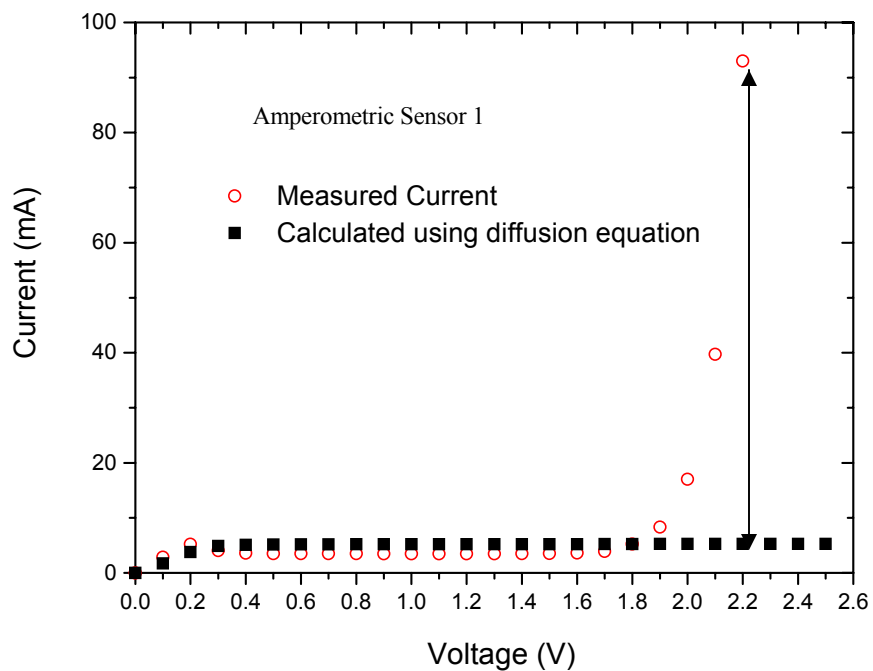
<u>Figure 8:</u> Measured current (open symbols) vs. applied voltage for amperometric sensor 1. Also plotted in the figure is the calculated current (filled symbols) based on the diffusion current equation. Note that beyond an applied voltage of ~1.9 V, the actual current rapidly rises, and is much greater than the calculated current. All this excess current is due either to the development of nonstoichiometry or decomposition. For example, the double arrow shows the excess current due to nonstoichiometry development and/or decomposition at an applied voltage of ~2.2 V.

$$\varphi(X)$$

$$\mu_{O_2}^{II} \quad p_{O_2}^{II}$$

V

Reference

$$\mu_{O_I}^{I}$$

$$\mu_{O_2}^{II} \quad p_{O_2}^{II}$$

Working

Counter

$$p_{O_2}^{I}$$

X

$$\tilde{\mu}_{O^{-2}}^{I}$$

$$\mu_{O_2}^{X} \quad \varphi^{X}$$
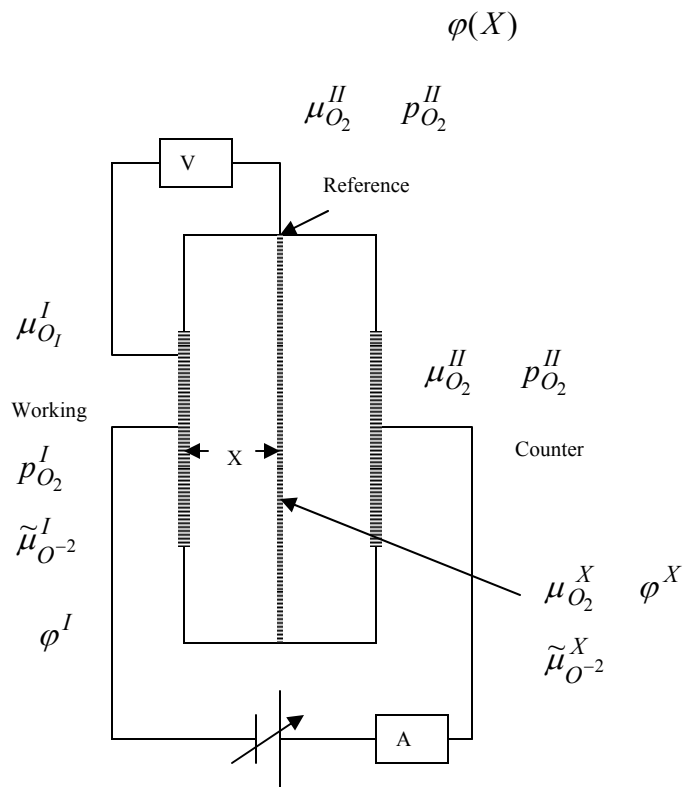
$$\varphi^{I}$$

$$\tilde{\mu}_{O^{-2}}^{X}$$

A

Figure 9: A schematic of the three electrode system, under an applied DC bias. The working electrode is a prospective cathode, which is porous and of a finite thickness. The net cathodic current is limited by the porosity, thickness, and the oxygen partial pressure. However, under an applied DC bias, the chemical potential of oxygen, μ_{O_2}, can be considerably lower, thus leading to local decomposition and/or the development of nonstoichiometry.
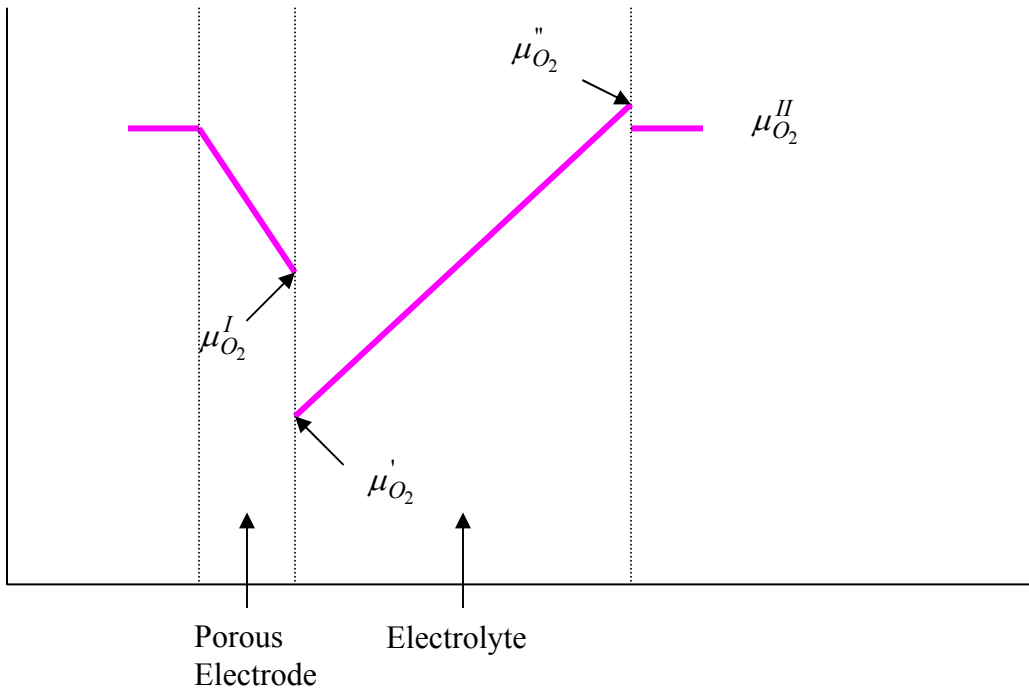
Figure 10: A schematic variation of the chemical potential of oxygen, μ_{O_2}, through the electrode (cathode) and the electrolyte of a three-electrode system often used for the study of electrode kinetics. If $\mu_{O_2}^{'}$ is low enough, either a nonstoichiometry will be developed or electrolyte decomposition may occur. In either case, this will be reflected as additional current, not attributable to the cathodic reaction. This effectively leads to an overestimation of electrocatalytic activity.

REFERENCES

1) T. Kenjo, S. Osawa, and K. Fujikawa, *J. Electrochem. Soc.*, **138** 349 (1991).
2) C. W. Tanner, K-Z. Fung, and A. V. Virkar, *J. Electrochem. Soc.*, **144** 21-30 (1997).
3) H. Deng, M. Zhou, and B. Abeles, *Solid State Ionics*, **74** 75 (1994).
4) I. V. Murygin, *Elektrokhimiya*, **23** [6] 740 (1987).
5) A. V. Virkar, J. Chen, C. W. Tanner, and J-W. Kim, *Solid State Ionics*, **131** 189 (2000).
6) F. Zhao, Y. Jiang, G-Y. Lin, and A. V. Virkar, pp. 501 in SOFC VII, edited by H. Yokokawa and S. C. Singhal, Electrochemical Society Publication, Pennington, NJ, (2001).
7) M. J. Verkerk, B. J. Middlehuis, and A. J. Burggraaf, *Solid State Ionics*, **6** 159 (1982).
8) X. Guo, *Solid State Ionics*, **81** 235-242 (1995).
9) X. Guo, *Solid State Ionics*, **99** 137-142 (1997).
10) J. Frenkel, p. 37 in 'Kinetic Theory of Liquids', Dover, NY (1946).
11) K. Lehovec, *J. Chem. Phys.*, **21** [7] 1123-1128 (1953).
12) K. L. Kliewer and J. S. Koehler, *Phys. Rev.*, **140** [4A], A1226-A1240 (1965).
13) K. L. Kliewer, *Phys. Rev.*, **140** [4A], A1241-A1246 (1965).
14) F. Zhao, T. Armstrong, and A. V. Virkar, *J. Electrochem. Soc.*, **150** [3] A249-A256 (2003).
15) X. Guo and J. Maier, *J. Electrochem. Soc.*, **148** [3] E121-E126 (2001).

LIST OF ACRONYMS AND ABBREVIATIONS

LSC: Sr-doped $LaCoO_3$
LSGM: Sr- and Mg-doped $LaGaO_3$
LSM: Sr-doped $LaMnO_3$
SDC: Samaria-Doped Ceria
SLP: Sintering and leaching process
SOFC: Solid oxide fuel cell
YSZ: Yttria-stabilized zirconia